A hybrid discrete bubble-lattice Boltzmann-discrete element model for gas-charged sediments

Min Wang[1], Y.T. Feng[2]*, Yong Wang[3], T.M. Qu[2], Wei He[4]

1 T-3 Fluid Dynamics and Solid Mechanics Group, Theoretical Division, Los Alamos National Laboratory, Los Alamos, New Mexico 87545, USA

2 Zienkiewicz Centre for Computational Engineering, College of Engineering, Swansea University, Swansea, Wales SA1 8EP, UK

3 State Key Laboratory of Geomechanics and Geotechnical Engineering, Institute of Rock and Soil Mechanics, Chinese Academy of Sciences, Hubei 430071 China

4 School of Civil Engineering and Architecture, Anhui University of Science and Technology, Anhui 232001, China

* Corresponding e-mail: y.feng@swansea.ac.uk

Abstract

This paper presents a hybrid discrete bubble-lattice Boltzmann-discrete element modelling framework for simulating gas-charged sediments, especially in the seabed. A discrete bubble model proposed in chemical engineering is adapted in the coupled discrete element/lattice Boltzmann method to model the migration of gas bubbles in saturated sediments involving interactions between gas bubbles and fluid/solid phases. Surface tension is introduced into the discrete bubble model in this work, so that it can handle the complex gas-fluid-solid interface. The discrete element and lattice Boltzmann methods are, respectively, employed to simulate fluid flows and mechanical behaviours of sediments. A velocity-interpolation based immerse boundary method is utilised to resolve the coupling between the fluid flow and the solid/gas phase. The proposed technique is preliminarily validated using simulations of bubble migration in fluids, which is followed by high-resolution investigations of the transport of a gas bubble in seabed sediments. It is demonstrated that this hybrid method can reproduce, to a certain degree, the characters of bubbles moving in seabed sediment tests.

Keywords

Discrete bubble model; Fluid-solid-bubble interaction; Lattice Boltzmann Method; Discrete Element Method; Bond model; Immersed Boundary Method

1 Introduction

With the rapid development of offshore constructions in China over the recent years, gas-charged sediments have been frequently encountered that could cause significant geochemical and

geotechnical consequences. The widespread distribution of undissolved gas within seabed sediments has also been found in many locations over the world [1]. Some commonly encountered geomechanical disasters include: 1) gas combustion and eruption caused by the blow-outs during drilling operations [2]; 2) the instability of offshore structures induced by the reduction of stiffness and strength due to the presence and transport of gas bubbles [3]; and 3) the instability of foundations due to the reduction of skin friction of the interface between foundations and sediments when gas bubbles migrate along the interface [4].

The occurrence and migration of undissolved gas, usually methane, has also a significant influence on the greenhouse effect. It was reported [5] that the release of bubbles from sediments, particularly wetland sediment, to the overlying water column constitutes large amount of atmospheric methane. Besides, bubble growth and movement in soft marine sediments are crucial steps in gas hydrate dynamics [6]. Therefore, understanding the presence of the gas bubble and its migration within sediments is of great importance for various disciplines and engineering practice.

Based on acoustic detection and scanning electron microscope studies, it was reported [7, 8] that the existence of gas bubbles in fine-grained clay and silt is quite different from bubbles in coarse-grained sand and gravel. The bubbles in fine-grained sediment are typically much larger than the normal void spaces, with each bubble forming a cavity within the soil structure; while in the coarse-grained soils, discrete bubbles are trapped within the pores formed by grains without distorting the soil structure and the size of these discrete bubbles is smaller than the void space. Wheeler [9] proposed a theoretical model to characterise the movement of gas bubbles in fine-grained sediments. It is found that the bubbles, in disc or spherical shape, whose size is larger than a critical size should have sufficient buoyancy to move upward under static loading conditions, and the critical bubble size is proportional to shear strength. These findings are validated by simple laboratory tests. From the laboratory injection tests performed by Etiope and Lombardi [10], gas through saturated sand was found moving up to ten times faster than gas in dry medium under the same injection pressure.

A model for the growth of methane bubbles in elastic sediments was developed using a reaction-diffusion theory coupled to a linear elastic fracture mechanics [11]. Then disc-shaped methane bubbles, resulted from growth in a medium that elastically resists expansion of the bubbles and yields by fracture, were modelled. It is found that both the growth rate and shape of a bubble in an elastic-fracturing sediment are dominated by the effects of fracturing events. Laboratory tests were carried out to investigate the effect of blow-outs on the foundation stability when the foundation is exposed to different static load directions and magnitudes [12]. Then, a finite element analysis in combination with linear elastic fracturing theory using software PLAXIS was performed to predict the gas flow paths.

The CT technique was introduced to investigate the migration of bubbles within shallow sediments in laboratory [13]. It is shown that bubbles are disc-shaped in soft muddy sediments, but are spherical away from mud contacts in sandy sediments. The muddy sediment responds as a fracturing elastic solid to bubble growth, whereas sands appear to act plastically. However, a recent CT study [14] reported different findings. The disc-like bubble development was not observed; instead, bubbles in

both clay and sand were either close to spherical or elongated. Johnson et al. [15] proposed an enhanced model to simulate gas migration within consolidated soft sediments. The lattice Boltzmann method (LBM) was used to simulate bubble flows in porous media whose interior void structure is constructed by the CT test. The Monte Carlo gas diffusion model was adopted to characterize the effective diffusivity through bubble networks.

Although some research work, including experiments, analytical solutions and numerical simulations, has been done to investigate the behaviour of complex gas-liquid-solid mixtures, relatively less attention has been paid to this research topic and the current understanding of the bubble migration mechanism in seabed sediments is still very limited. Particularly, the above-mentioned models do not consider the full coupling among gas bubbles, solid particles and fluid flows from the viewpoint of geomechanics. Because the transportation of gas bubbles occurs at the grain/pore level, the surface tension applied at the interface of three phases needs to be carefully resolved and the rearrangement of solid particles caused by moving bubbles plays an important role in the strength reduction of sediments.

The aim of this work is to develop a high-resolution model, where the complex gas-fluid-solid interaction can be handled, for simulating the bubble transport within sediments based on our previous work [16, 17]. In this hybrid technique, a discrete bubble model will be adopted to describe the movement and growth of gas bubbles; the lattice Boltzmann method combined with an immersed boundary method will be used to solve the pore fluid flow, the interaction of fluid-solid particles and the interaction of fluid-gas bubbles; the discrete element method (DEM) will be employed to simulate the sediment deformation, and the capillary force resulted from the surface tension applied at the three-phase interface will be incorporated.

The rest of this paper is organised as follows: In Section 2, a discrete bubble model for gas bubbles will be introduced first. For the sake of completeness and simplification, a brief description of both DEM and LBM is also provided in the section. Then, fluid-solid, fluid-gas and gas-solid couplings are described in Section 3, which is followed in Section 4 by illustrative simulations of bubble migration in fluids and the transport of gas bubbles in seabed sediments.

2 Methodologies

2.1 Discrete bubble model

A discrete bubble model [18] was first proposed in chemical engineering to simulate the dynamics of dispersed bubbles in fluids. In this model a gas bubble is considered as spherical and non-deformable. The movement of each bubble is governed by Newton's second law (see Eq. 1) and the position of the bubble is updated through an explicit time-stepping algorithm.

$$m\frac{dv}{dt} = F_{total} \tag{1}$$

where m is the mass of the bubble; v is the bubble velocity; F_{total} is the resultant force applied to the bubble and it will be described in detail below.

The same model was adopted by Tomiyama et al. [31, 32] with partial modification to the drag, lift and wall force closures. Detailed discussion about these forces can be found in [33]. Then, bubble break-up and coalescence are incorporated to recover more complicated phenomena [19]. The bubble coalescence model was proposed by Sommerfeld et al. [34] which is extensively used later to determine if the collision will result in coalescence or not by other researchers. Bubble coalescence is incorporated by comparing the contact time with the film drainage time. If the film drainage time is less than the bubble contact time, coalescence takes place. Such implementation of bubble coalescence has been used by Darmana et al. [35] and Lau et al. [36]. Another complex property of bubbles in fluid is the breakup nature. It is simulated by researchers [36, 37].

In this work, the discrete bubble model without bubble break-up and coalescence is employed and we enhance it by accounting for the capillary force caused by surface tension at the three-phase interface and the interaction of bubble and solid. The ingredients of the resultant force applied to a bubble are given below

$$F_{total} = F_G + F_B + F_f + F_D + F_C \tag{2}$$

F_G -- Gravity;

F_B -- Buoyancy force;

F_f -- Hydrodynamic forces;

F_D -- Detachment force caused by bubble-solid collision or bubble-bubble collision;

F_C -- Capillary force.

The hydrodynamic forces will be calculated by the immersed boundary method, and the detachment force (see Fig. 1) will be determined by the contact mechanics, details of these two forces will be given in Section 3.

The capillary forces (shown in Fig. 1) for 2D and 3D models can be derived through integrating the component T_{sy} (which is in the normal contact direction) of surface tension over the three-phase interface. Due to symmetry of the component T_{sx}, its contribution to the total force is zero. They are, respectively, given by

$$F_C = 2R_p T_s \sin\phi \sin(\theta - \phi) \tag{3}$$

$$F_C = 2\pi R_p T_s \sin\phi \sin(\theta - \phi) \tag{4}$$

where T_s is the surface tension and it is selected as 0.0756 N/m corresponding to 0 Celsius; θ and ϕ are angles defined in Fig. 1; and R_p and R_b are the radii of solid particles and gas bubbles respectively.

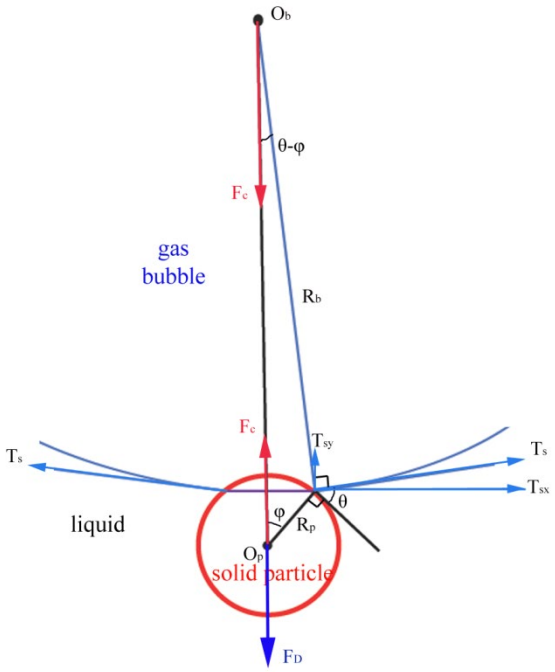

Fig. 1 Capillary force caused by surface tension

With the upward movement, the gas bubble will grow up but keep the same shape (disc for 2d cases and sphere for 3D cases). The real-time volume can be updated by the equation of state

$$\frac{P_1 V_1}{T_1} = \frac{P_2 V_2}{T_2} \tag{5}$$

where P is the hydrostatic pressure; V is the volume of the bubble; and T is the temperature. An isothermal condition is assumed in the current work.

2.2 Lattice Boltzmann method

The lattice Boltzmann method is a modern numerical approach in Computational Fluid Dynamics. In LBM the fluid domain is divided into regular lattices and the fluid phase is represented by a group of (imaginary) fluid particle packages resided at each lattice node. Each particle package includes several particles, such as 9 particles in the commonly used D2Q9 model. The fluid flow can be achieved through resolving the particle collision and streaming processes, and the lattice Boltzmann equation (LBE) is used to solve the streaming and collision processes of fluid particles. The primary variables of LBM are the so-called fluid density distribution functions, which are portions of the fluid

density, associated with the fluid particles. Both mass and momentum of fluid particles are characterised by the fluid density distribution functions. The detail of LBM can be referred to [16].

The lattice Boltzmann equation is described by

$$f_i(x + e_i \Delta t, t + \Delta t) - f_i(x,t) = \Omega_i \tag{6}$$

where f_i is the fluid density distribution function in *i* direction; x and e_i are the coordinates and velocity vectors at the current lattice node; t and Ω_i are, respectively, the current time and the collision operator.

In the single relaxation lattice BGK Model [20], Ω_i is characterised by a relaxation time τ and the equilibrium distribution functions $f_i^{eq}(x,t)$.

$$\Omega_i = -\frac{\Delta t}{\tau}\left[f_i(x,t) - f_i^{eq}(x,t)\right] \tag{7}$$

In this work, the D2Q9 model is adopted, and $f_i^{eq}(x,t)$ are defined as:

$$f_i^{eq} = \omega_i \rho(1 + \frac{3}{C^2} e_i \cdot v + \frac{9}{2C^4}(e_i \cdot v)^2 - \frac{3}{2C^2} v \cdot v) \qquad (i = 0,...,8) \tag{8}$$

where ρ and v are the macroscopic fluid density and velocity, respectively. ω_i are the weighting factors:

$$\omega_0 = \frac{4}{9}, \qquad \omega_{1,2,3,4} = \frac{1}{9}, \qquad \omega_{5,6,7,8} = \frac{1}{36} \tag{9}$$

The macroscopic fluid density ρ and velocity u can be calculated from the distribution functions

$$\rho = \sum_{i=0}^{8} f_i, \qquad \rho u = \sum_{i=1}^{8} f_i e_i \tag{10}$$

The fluid pressure is given by

$$P = C_S^2 \rho \tag{11}$$

where C_S is termed the fluid speed of sound, defined as $C_S = h/(\sqrt{3}\Delta t)$, where h is the lattice spacing and Δt is time step.

2.3 Discrete element method

The discrete element method for geomechanical problems treats the geomaterial as a collection of discrete particles. Through modelling the interaction of particles in contact and the consequent particle movement, the macroscopic behaviour of geomaterials can be recovered.

The motion of a particle is governed by Newton's second law

$$ma + cv = F_c + F_f + F_C + mg \tag{12}$$

$$I\ddot{\theta} = T_c + T_f \tag{13}$$

where m and I are respectively the mass and the moment of inertia of the particle; c is a damping coefficient; a and $\ddot{\theta}$ are the acceleration and angular acceleration respectively; F_c and T_c are the (resultant) contact force (including interactions caused by solid particle collision and between gas bubble and solid particle collision) and the corresponding (resultant) torque respectively; F_f and T_f are the (resultant) hydrodynamic force and the corresponding (resultant) torque respectively.

As mentioned before, F_C is the capillary force. Because the shape of both solid particles and gas bubbles are assumed circular in the current work, the capillary force will pass through the centroid of the particle and make no contribution to rotation.

The solid particle interaction consists of the interaction between unbonded particles and the bonded particle interaction simulated by bond models. As the unbounded particle interaction independent of bond is well known in granular mechanics, it will not be described here and the detailed introduction can be found in our previous work [16].

Bond models have been incorporated into DEM and extensively investigated in geomechanics [30]. They are employed to simulate the cohesion of bonded particles. The bond model adopted in this work is proposed by Wang et al. [21, 22]. It includes a normal bond, accounting for the softening effect, and a history dependent Coulomb friction model. Its normal force F_n^b and tangential force F_t^b are given by

$$F_n^b = \begin{cases} K_n^b \delta & \delta >= \delta_1 \\ K_n^b \delta_1 + K_{sf}(\delta - \delta_1) & \delta_2 < \delta < \delta_1 \\ 0 & \delta < \delta_2 \end{cases} \tag{14}$$

$$F_t^b = -\frac{\dot{\delta}_t}{\left|\dot{\delta}_t\right|} \begin{cases} K_t^b \left|\delta_t\right|; & \left|K_t^b \delta_t\right| \le \mu F_n^b \\ \mu F_n^b; & \left|K_t^b \delta_t\right| > \mu F_n^b \end{cases} \tag{15}$$

where K_n^b and K_t^b are the normal stiffness and tangential stiffness for the bond or cement respectively; F_{bn} is the critical tensile force and F_{bt} is critical shear strength; K_{sf} , δ_1 and δ_2 are, respectively, the stiffness for the softening period, the overlap corresponding to the critical bond force and the overlap corresponding to the bond breakage; and μ is the coefficient of friction.

The torque applied to an unbonded particle can be calculated by the tangential force. However, for a bonded particle, in addition to the torque contributed by tangential forces, the torque caused by the relative rotation between two bonded particles should be considered and given by

$$T_c^b = -k_n^b I \Delta\theta \tag{16}$$

where $\Delta\theta$ is the relative rotational angle of two bonded particles.

3 Multiphase Coupling

3.1 Fluid-solid and gas-fluid couplings

Fluid-solid and gas-fluid couplings are achieved by the immersed boundary method (IBM) proposed by Dash et al., [23]. In this IBM-LBM framework, the LBE which governs the evolution of fluid particles is modified by introducing a body force term *F* into Equation 6

$$f_i(x + e_i \Delta t, t + \Delta t) - f_i(x,t) = \Omega_i + F_i \Delta t \tag{17}$$

where

$$F_i = (1 - \frac{1}{2\tau}) w_i (\frac{e_i - u}{C_S^2} + \frac{e_i \cdot u}{C_S^4}) \cdot \mathrm{f} \tag{18}$$

and f is the force density at the lattice node.

The corresponding fluid velocity is modified by the force density as

$$\rho u = \sum_{i=1}^{8} f_i e_i + \frac{1}{2} \mathrm{f} \Delta t \tag{19}$$

In this scheme (see Fig. 2), the solid and/or bubble boundaries are discretised into several Lagrangian boundary points. At each time step, the primary steps involved are described as follows:

1) Calculate the velocities of boundary points of each particle through rigid body motion;
2) Calculate the fluid velocity at the same boundary node through the interpolation of neighbouring fluid nodes using Dirac delta distribution functions;
3) Compute the difference (so-called velocity correction, δU_b) between the interpolated boundary velocity and the velocity of the boundary point;
4) The velocity correction of each boundary point is then distributed to its surrounding fluid nodes using the following equation

$$\delta U(x_{ij}, t) = \sum_k \delta U_b(x_b^k, t) \cdot D(x_{ij} - x_b^k) \cdot \Delta s_k \tag{20}$$

where x_{ij} and x_b^k are the coordinates of fluid nodes and boundary points respectively, k is the serial number of boundary points related to the fluid nodes and Δs is the arc length between two consecutive boundary points. $D(\cdots)$ is the Dirac delta function.

5) The velocity and density force at the lattice node are calculated by

$$u(x_{ij},t) = u(x_{ij},t) + \delta U(x_{ij},t) \tag{21}$$

$$\mathrm{f} = \mathrm{f} + \frac{2\rho\delta U(x_{ij},t)}{\Delta t} \tag{22}$$

6) The hydrodynamic force applied to the boundary point can be computed

$$F_b(x_b,t) = F_b(x_b,t) + \frac{2\rho\sum_k \delta U_b(x_b^k,t)}{\Delta t} \tag{23}$$

7) Repeat steps 2) to 6) for each boundary node until the velocity correction is sufficiently small.

8) Finally, update the fluid density distribution functions using Equations 17 and 18.

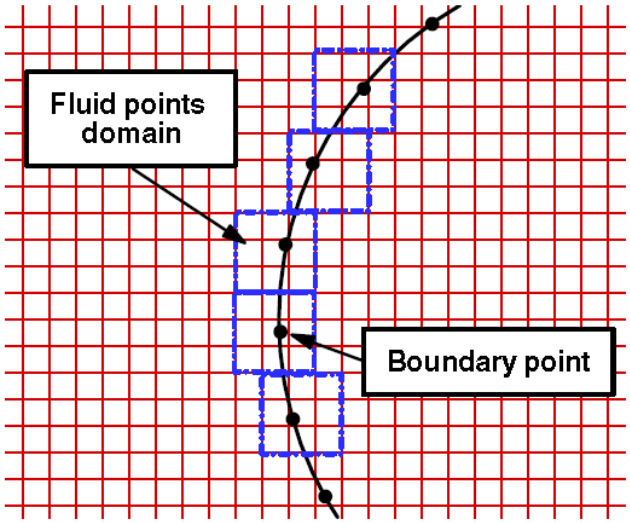

Fig. 2 Interpolation-based moving boundary scheme (after [24])

3.2 Gas-solid coupling

The gas-solid coupling is achieved by the capillary force F_C and the pressure inside the gas bubble that causes the detachment force F_p. The expressions of the detachment force for 2D and 3D problems are, respectively, given by [26]

$$F_p = \frac{4T}{R_b}\pi R_p \sin(\varphi) \qquad \text{(2D)} \tag{24}$$

$$F_p = \frac{2T}{R_b}\pi R_p^2 \sin^2(\varphi) \qquad \text{(3D)} \tag{25}$$

The definition of the relevant parameters can be found in Fig. 1.

In this work, the detachment force calculated by the above equation is found too small to push the gas bubble and the neighbouring solid particles apart from each other. Because the shallow gas is normally buried around 1000 m in depth [25], gas bubbles can be treated as special particles with certain stiffness compared to the atmospheric gas. When a gas bubble collides with a solid particle, their contact force can be calculated by theoretical contact modes in contact mechanics which have been extensively used to handle the interaction between particles in DEM. The proposed linear contact model is given by

$$F_p = \alpha k_n \delta_{bp} \tag{26}$$

where α is a reduction coefficient; k_n is the stiffness of solid particles, and δ_{bp} is the overlap between the gas bubble and solid particle in contact.

When the three-phase contact is formed, the capillary force caused by the surface tension can be calculated by Equations 3 and 4.

4 Numerical Examples and Discussions

4.1 Migration of gas bubbles in fluid

First, to validate the gas-fluid coupling, a numerical model of the migration of two bubbles in a water-filled tube is carried out. The size of the tube is 3 cm diameter (in the X-direction) by 6 cm height (in the Y-direction). The fluid domain is divided into 150 × 300 square lattices with spacing h=0.2 mm. The kinematic viscosity and density of the fluid are 10^{-6} m^2/s and 1000 kg/m^3, respectively. The density of the gas bubbles is selected as 100 kg/m^3, because the shallow gas is normally buried hundreds of meters below the sea. Their radius is 0.1 cm. Four boundaries of the model are stationary walls and thus the no-slip boundary condition is imposed for the fluid. Initially, two stationary gas bubbles are generated at two positions (1cm, 0.3cm) and (2cm, 0.3cm). Due to buoyancy force, the bubbles will move upward gradually. In this simulation, the immersed boundary method [23] is employed to resolve the bubble-fluid interaction. The bubble surface is divided into 20 boundary points. The relaxation time (τ) is selected as 0.5001, and the time step is 1.333×10^{-6} s.

The positions of the bubbles and the velocity contours of the fluid at different time instants, 0.0s, 0.667s, 1.33s, 2.0s, 2.67s, 3.17s, are depicted in Fig. 3. It can be found that both the movement of the two bubbles and the fluid velocity contour display symmetric characteristics along the vertical middle line. For the two bubbles, the time evolution of the particle velocity and position in the vertical direction are respectively compared in Figs. 4-6. Figs. 4 & 5 show that both bubbles are moving upward. In the meantime, they are oscillating in the horizontal direction but in a symmetric manner. Figure 6 shows the variation of the radii of these two bubbles over time. It is found that the radii of the two bubbles increase simultaneously with the same magnitude, because their movement in the vertical direction is the same. When they move upward, the hydrostatic pressure decreases, then the volume increases based on the equation of state in Eq. 5. Fig. 7 gives the variation of the horizontal velocities of the two bubbles. Their velocities in the X direction are symmetric, which can explain the result observed in Fig.

4. From the above observation, it can be concluded that the discrete bubble model and the IBM-LBM appears to capture the behaviour of the bubble-fluid system well.

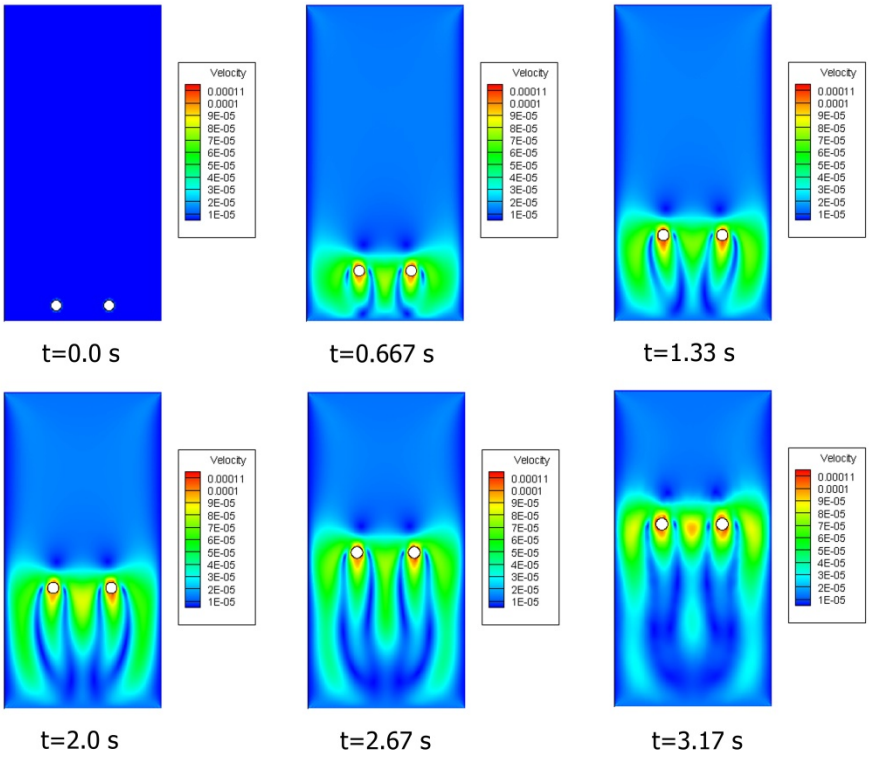

Fig. 3 Snapshots of bubble migration in fluid

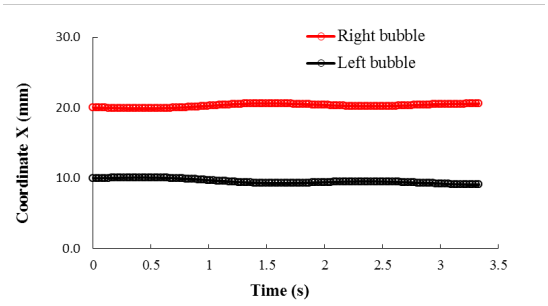

Fig. 4 Horizontal bubble positions versus time

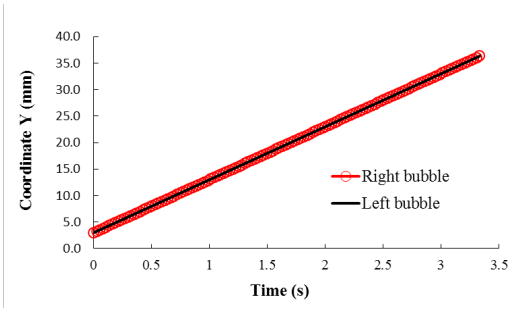

Fig. 5 Vertical bubble positions versus time

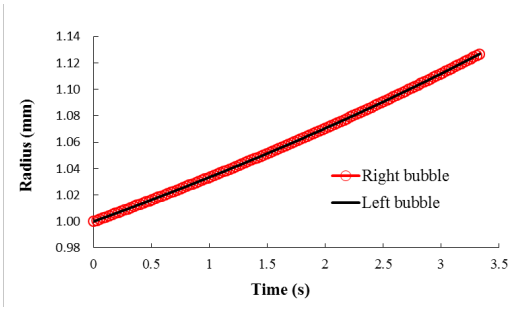

Fig. 6 Change of bubble sizes over time

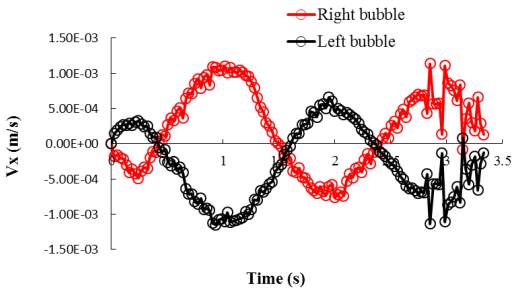

Fig. 7 Variation of horizontal bubble velocities

4.2 Migration of gas bubbles in saturated sediments

In this section, the proposed discrete bubble-lattice Boltzmann-discrete element model will be employed to investigate the migration of gas bubbles in both saturated sand and silt.

As the proposed technique is a high-resolution model, which aims at resolving the complex multiphase coupling at the pore/grain scale, only small-scaled models, which can be envisioned as the representative elementary volume (REV) of real sediments, are set up.

a) Coarse-grained sediment model

The numerical model (0.1 m × 0.1 m) is divided into 500 × 500 square lattices with spacing h=0.2 mm. The parameters of the fluid and the gas bubble are the same as those in the previous simulation except for the bubble size. Because the gas bubble normally exists within the pores formed by sandy particles, the initial radius of the gas bubble is selected as 1.5 mm, which is smaller than the average size of sandy particles. The bubble surface is divided into 20 boundary points. The relaxation time (τ) is select as 0.50001, and the time step is 1.333×10^{-7} s. The coarse-grained sediment is represented by a collection of 527 sandy particles, whose size distribution ranges from 1.5 to 2.5 mm. Their normal and tangential stiffnesses are, respectively, 5×10^{7} N/m and 2×10^{5} N/m. Critical normal and tangential bond strengths are 5 and 2.5 N. It is known that the pore space can be closed in 2d DEM simulations. Normally when the fluid is coupled with 2D DEM, a hydraulic radius (a factor smaller than 1.0) is applied to the real particle size so that a flow path can be considered [17]. For the contact force in the solid part, the particle size is not changed. Four boundaries of the model are stationary walls and thus the no-slip boundary condition is imposed for the fluid. Initially, the gas bubble shown in Fig. 8 is generated. In order to better observe movement of the gas bubble and the rearrangement of sandy particles, sediments located in different regions are distinguished by white and black colours, respectively.

In practical engineering, the movement of gas bubbles is triggered by unloading caused by underground excavation, which will apply an upward acceleration to bubbles, as shown in the previous bubble-fluid model. Because the proposed technique is very computationally expensive, a relatively large velocity is applied to each gas bubble to accelerate the simulation in these two models.

However, if the velocity is not very large, the observed phenomenon should be similar, which can be proved from the following simulations.

Fig. 8 gives the snapshots of simulations at different time instants, 0.027 s, 0.053 s, 0.08 s, 0.107 s and 0.133 s. To distinguish between the gas bubble and the sandy particles, the gas bubble is marked in yellow. The colour bar shows the magnitude of fluid velocity. During the whole simulation, the gas bubble slowly moves upward, and pushes away sandy particles on the way. Then, the surrounding sandy particles rearrange their positions and refill the space that the bubble leaves. From Fig. 9, it is found that during the upward movement of the bubble it oscillates in the horizontal direction at the same time. Figs. 10 and 11 show the variation of the horizontal velocity and the bubble size over time. The horizontal velocity shifts the direction around 0.03 s and 0.06 s, which correspond to the valley and peak observed in Fig. 9. Besides, the bubble size increases gradually when the bubble moves upward.

The variation of the hydrodynamic force applied on the bubble in the vertical direction is given in Fig. 12. It is seen that the vertical hydrodynamic force is opposite to the direction of vertical movement, and its magnitude almost periodically varies between -14 N and 0 N.

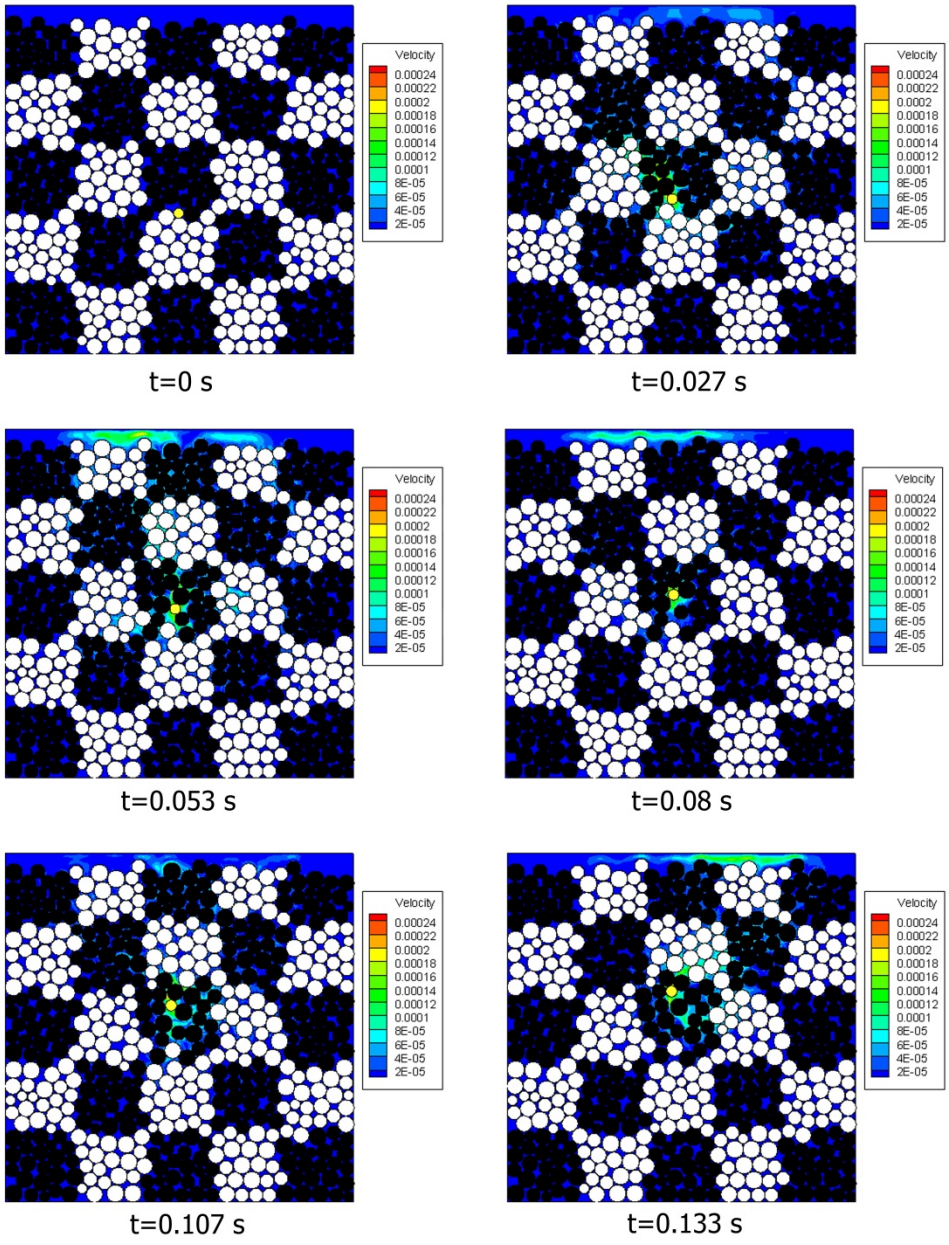

Fig. 8 Snapshots of bubble migration in sand

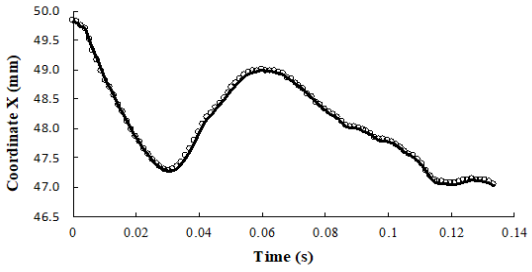

Fig. 9 Variation of horizontal bubble position in

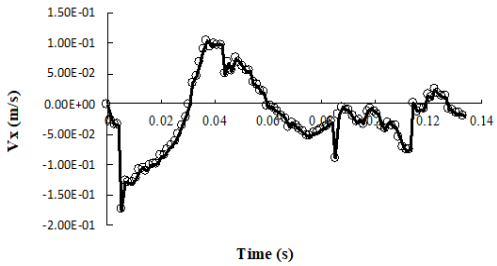

Fig. 10 Variation of horizontal bubble velocity in

sand

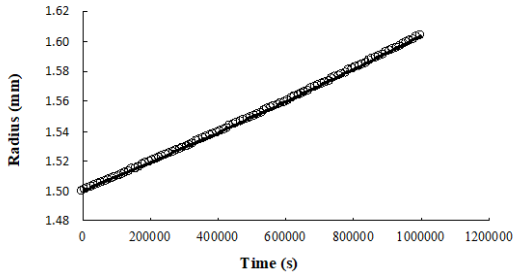

Fig. 11 Variation of bubble size in sand

sand

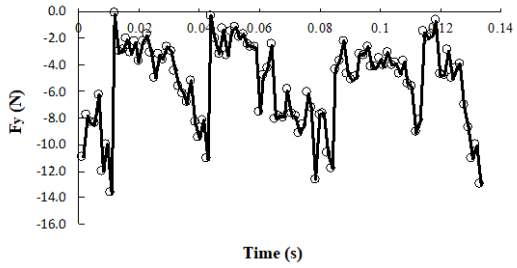

Fig. 12 Variation of vertical hydrodynamic force applied on the bubble in sand

b) Fine-grained sediment model

The numerical model (1 mm × 2 mm) is divided into 100 × 200 square lattices with spacing h=0.01 mm. The bubble surface is divided into 20 boundary points. The relaxation time τ is selected as 0.50001, and the time step is set to be 3.333×10^{-6} s. The fine-grained sediment is represented by a collection of 823 silty particles, whose size distribution ranges from 0.015 to 0.025 mm. The normal and tangential stiffness of unbounded particles is, respectively, 5×10^{7} N/m and 2×10^{5} N/m, and The normal and tangential stiffness of bounded particles is, respectively, 5×10^{6} N/m and 10^{5} N/m. Based on some published reports [7, 8], the size of gas bubbles is much larger than that of silty particles, so the radius of the gas bubble in the model is selected as 0.08 mm. The cohesion between silty particles is simulated by a bond model with strain softening. The detailed introduction of the adopted bond model can be found in our previous work [22, 27]. Four boundaries of the model are stationary walls and thus the no-slip boundary condition is imposed. At the beginning the gas bubble shown in Fig. 13 is generated. In order to better observe movement of the gas bubble and the silty particles, sediments located in different regions are distinguished by white and black colours, respectively. In addition, the bond existing between a pair of bonded particles is represented by a red link connecting the two particle centres.

Snapshots of simulations at different time instants are shown in Fig. 13. It is found that with the upward movement of the gas bubble, the silty particles above the bubble moves as a whole due to the effect of cohesion. From the third snapshot at 1.33 s, obvious cracks where the bond is broken can be observed. Cracks further develop with time. An interesting phenomenon is that when the gas bubble passes through fine-grained sediments, it creates an apparent fracture which is not filled by sediment particles due to cohesion between bonded particles. This phenomenon was also reported by other researchers [5]. The variations of the horizontal position, velocity in the X direction and bubble size of the gas bubble are shown in Figs. 14, 15 and 16, respectively. Their trends are similar to those in the above coarse-grained sediment model. Fig. 17 illustrates that the hydrodynamic force applied on the

bubble in fine-grained sediments is much smaller than the one in coarse-grained sediments, and the magnitude of oscillation is also very small.

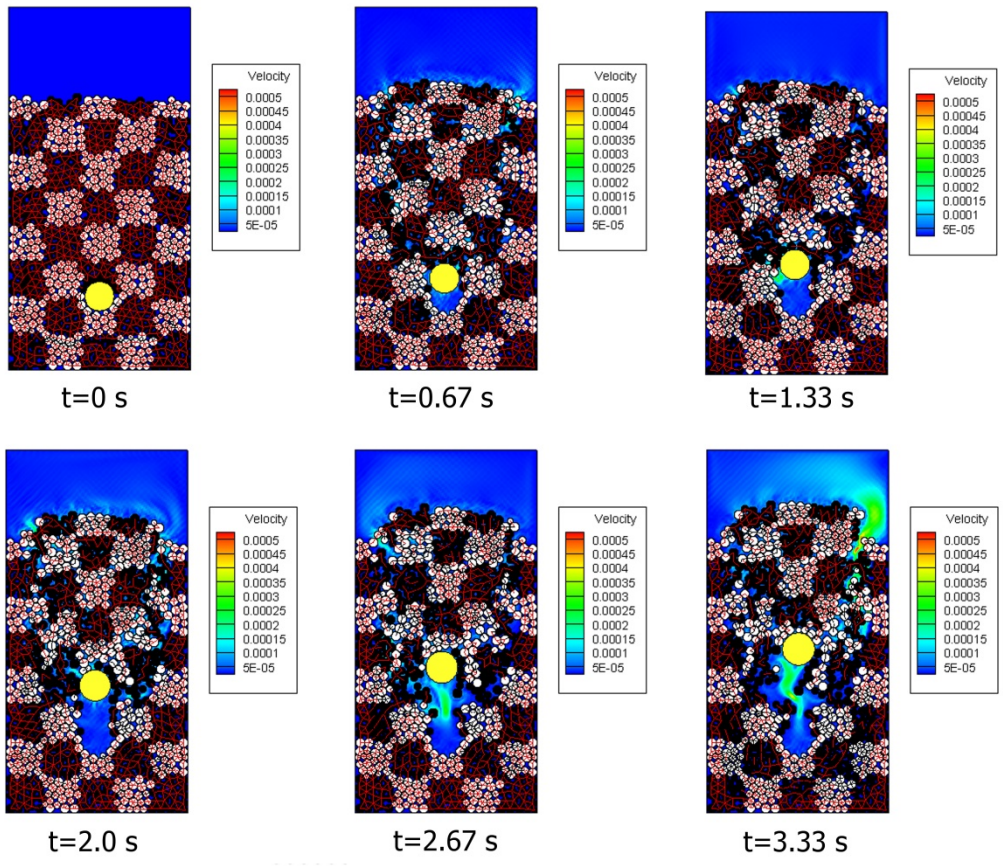

Fig. 13 Snapshots of bubble migration in silt

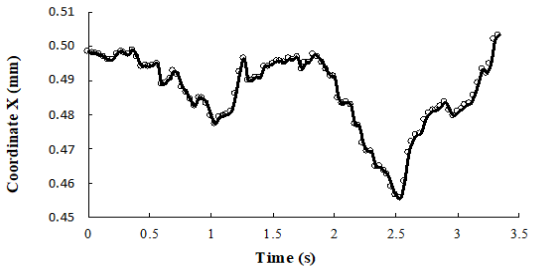

Fig. 14 Variation of horizontal bubble position in silt

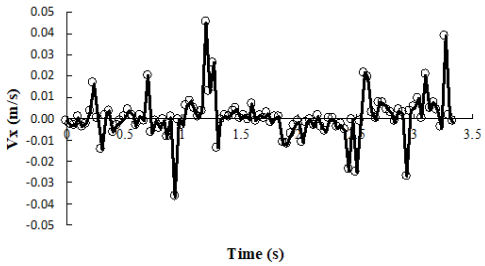

Fig. 15 Variation of horizontal bubble velocity in silt

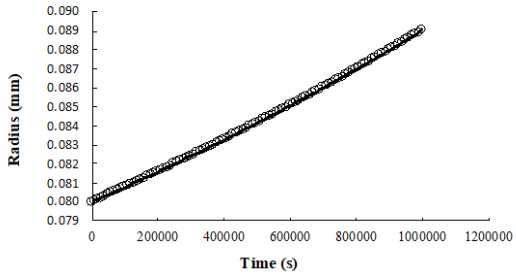

Fig. 16 Variation of bubble size in silt

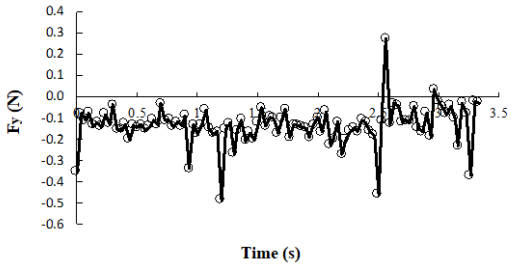

Fig. 17 Variation of vertical hydrodynamic force applied on the bubble in silt

4.3 Discussions

The occurrence of gas bubbles in coarse-grained and fine-grained sediments is reported to be significantly different. Bubbles in coarse-grained sediments are trapped within the pores formed by grains without distorting the soil structure and the size of these discrete bubbles is smaller than the void space. In contrast, in the fine-grained soils discrete bubbles are typically much larger than normal void spaces and grain size, with each bubble forming a cavity within the soil structure. This is the reason how the pore size is selected in the previous two samples shown in Figs. 8 and 13.

It is observed that once the gas bubble starts migrating upward the sand particles above the bubble will move together. Then, the sand particles are pushed away and forms a path for the gas bubble to pass through. When the gas bubble passes, the sand particles will redeposit and fill the void left by the bubble.

However, it is found that with the upward movement of the gas bubble in the fine-grained sediment fractures initiate from the bubble surface along left-top and right-top directions, and the fractured part will move as a whole. No particle reposition can be seen. This observation matches other researchers report and can be confirmed by our laboratory tests shown in Fig. 18. The laboratory sample is prepared using silicon powder. A high precision industrial CT is used to scan the samples in different gas injection stages. Upswept fractures are captured during gas injection. Due to the cohesion among fine particles, fractured parts move together.

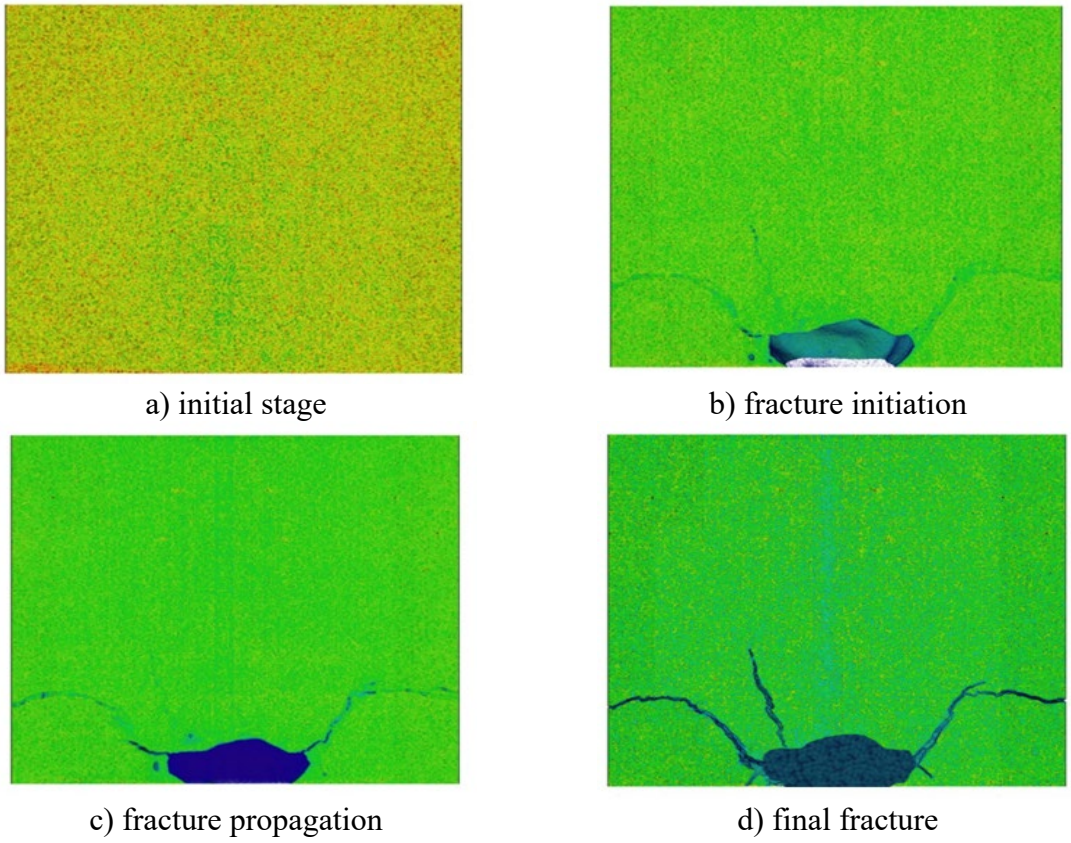

Fig. 18 Experimental results for bubble-induced fracture in the fine-grained sediment

The proposed technique is classified as a microscopic method. It solves the coupling among three phases at the grain level and surface tension is directly applied to their interface. Due to the microscopic nature it provides an insight to the real migration path of gas bubbles and local deformation of sediments around the bubble.

The information of the computer used is 1) Processor: Intel Core i5-2450 CPU@2.50GHz; 2) Memory: 6.00 GB. The computing cost of coarse-grained and fine-grained sediments models is respectively 2 h 58m 50 s and 15 h 29 m 42 s.

Compared with existing continuum methods, its computing cost is very high, and the spatial dimension of numerical models under investigation is very small. Besides, the bubble shape is always circular for 2D simulations. To better simulate the gas-fluid-particle system, complex bubble shapes will be considered later. However, a notable advantage of the current methodology is that not many assumptions and approximated treatments are required to make for three-phase coupling, while such coupling, together with real deformation and cracking, demands considerable efforts in continuum methods. For example, the path that bubbles pass through will generate a fracture in fine-grained sediments and should not be buried by fine grains. This phenomenon is generally more difficult to be handled by continuum-based methods.

It should be highlighted that the commonly used immersed moving boundary (IMB) scheme [28,29] is found non-convergent in three phase coupling. Further investigating into this issue reveals that the fluid density term in the collision operator which is proposed for solving liquid-solid coupling caused instability issues. When the density is below 100 kg/m^3, the nonconvergence appears. Therefore, the immersed boundary method is adopted in this work.

5 Conclusions

In this work, a discrete bubble model proposed in chemical engineering is enhanced and incorporated into the coupled discrete element-lattice Boltzmann method. Thus the migration of gas bubbles in saturated sediments involving interactions between bubbles and fluid/solid phases can be simulated at the grain/pore level. A velocity-interpolation based immerse boundary method is adopted to resolve the coupling between the fluid field and the solid/gas part. Then, qualitative validations of the proposed technique are carried out by high-resolution simulations of bubble migration in fluids, followed by investigations of the transport of a gas bubble in seabed sediments. Primary conclusions can be drawn as follows:

1) The proposed technique provides an insight into bubble transport in sea bed sediments through adding the capillary action to conventional discrete bubble models.

2) It can capture the real migration path of gas bubbles and subsequent mechanical responses of two different sediments. In fine-grained sediments the fracturing process and macroscopic mechanical behaviour can be easily reproduced by a simple bond model.

3) The adopted velocity-interpolation based immerse boundary method is capable of resolving the interaction between bubbles and fluids. In contrast, the commonly used immerse moving method suffers from a non-convergent issue due to the existence of the fluid density term in the collision operator.

4) This hybrid technique is promising for investigating the mechanism of mechanical response of gas charged sediments, like the wave attenuation in acoustic detection tests.

However, the proposed computational framework in the present work is only a preliminary attempt to address an important but very complex three phase interaction problem and many aspects of the methodology can be further improved and enhanced. Currently only disc-like bubbles are considered, and thus the real deformation of gas bubbles cannot be simulated yet. Another approximation which should be enhanced is the treatment of the bubble-solid interaction. It is found that the reported methods for the bubble-solid interaction in the conventional discrete bubble model yield very small forces, which will cause unrealistic overlap between gas bubbles and solid particles. The adopted bubble-solid interaction approach, which treats the gas bubble as a soft material with certain stiffness, is borrowed from contact mechanics for solid. Future work will focus on developing deformable bubble models and more accurate coupling methods between gas bubbles and solid particles.

Conflict of interest statement

On behalf of all authors, the corresponding author states that there is no conflict of interest.

References

[1] Fleischer, P., Orsi, T., Richardson, M. and Anderson, A., 2001. Distribution of free gas in marine sediments: a global overview. Geo-Marine Letters, 21(2), pp.103-122.

[2] Wang, Y., Kong, L., Wang, Y., Wang, M. and Cai, K., 2017. Deformation analysis of shallow gas-bearing ground from controlled gas release in Hangzhou Bay of China. International Journal of Geomechanics, 18(1), p.04017122.

[3] Sills, G.C. and Wheeler, S.J., 1992. The significance of gas for offshore operations. Continental Shelf Research, 12(10), pp.1239-1250.

[4] Wheeler, S.J., 1990. Movement of large gas bubbles in unsaturated fine-grained sediments. Marine Georesources & Geotechnology, 9(2), pp.113-129.

[5] Algar, C.K., Boudreau, B.P. and Barry, M.A., 2011. Initial rise of bubbles in cohesive sediments by a process of viscoelastic fracture. Journal of Geophysical Research: Solid Earth, 116(B4).

[6] Bratton, J.F., 1999. Clathrate eustasy: Methane hydrate melting as a mechanism for geologically rapid sea-level fall. Geology, 27(10), pp.915-918.

[7] Gardner, T.N. and Goringe, M.J., 1988. The measurement of gas bubble size distributions in a three phase laboratory gassy soil. Geotechnical Testing Journal, 11(1), pp.49-55.

[8] Sills, G.C., Wheeler, S.J., Thomas, S.D. and Gardner, T.N., 1991. Behaviour of offshore soils containing gas bubbles. Geotechnique, 41(2), pp.227-241.

[9] Wheeler, S.J., 1990. Movement of large gas bubbles in unsaturated fine-grained sediments. Marine Georesources & Geotechnology, 9(2), pp.113-129.

[10] Etiope, G. and Lombardi, S., 1996. Laboratory simulation of geogas microbubble flow. Environmental Geology, 27(3), pp.226-232.

[11] Gardiner, B.S., Boudreau, B.P. and Johnson, B.D., 2003. Growth of disk-shaped bubbles in sediments. Geochimica et Cosmochimica Acta, 67(8), pp.1485-1494.

[12] Gylland, A.S. and de Vries, M.H., 2008. The effect of gas blow-out on shallow offshore foundations. In Proceedings of the Second British Geotechnical Association International Conference on Foundations (ICOF 2008), Vol. 1, pp. 885-896.

[13] Boudreau, B.P., Algar, C., Johnson, B.D., Croudace, I., Reed, A., Furukawa, Y., Dorgan, K.M., Jumars, P.A., Grader, A.S. and Gardiner, B.S., 2005. Bubble growth and rise in soft sediments. Geology, 33(6), pp.517-520.

[14] Liu, L., De Kock, T., Wilkinson, J., Cnudde, V., Xiao, S., Buchmann, C., Uteau, D., Peth, S. and Lorke, A., 2018. Methane bubble growth and migration in aquatic sediments observed by X-ray μCT. Environmental science & technology, 52(4), pp.2007-2015.

[15] Johnson, M., Peakall, J., Jia, X., Fairweather, M., Harbottle, D., Biggs, S. and Hunter, T.N., 2018. Enhanced gas migration through permeable bubble networks within consolidated soft sediments. AIChE Journal, 64(11), pp.4131-4147.

[16] Wang, M., Feng, Y.T. and Wang, C.Y., 2016. Coupled bonded particle and lattice Boltzmann method for modelling fluid–solid interaction. International Journal for Numerical and Analytical Methods in Geomechanics, 40(10), pp.1383-1401.

[17] Wang, M., Feng, Y.T. and Wang, C.Y., 2017. Numerical investigation of initiation and propagation of hydraulic fracture using the coupled Bonded Particle–Lattice Boltzmann Method. Computers & Structures, 181, pp.32-40.

[18] Delnoij, E., Lammers, F.A., Kuipers, J.A.M. and van Swaaij, W.P.M., 1997. Dynamic simulation of dispersed gas-liquid two-phase flow using a discrete bubble model. Chemical engineering science, 52(9), pp.1429-1458.

[19] Jain, D., Kuipers, J.A.M. and Deen, N.G., 2014. Numerical study of coalescence and breakup in a bubble column using a hybrid volume of fluid and discrete bubble model approach. Chemical Engineering Science, 119, pp.134-146.

[20] Qian, Y.H., d'Humières, D. and Lallemand, P., 1992. Lattice BGK models for Navier-Stokes equation. EPL (Europhysics Letters), 17(6), p.479.

[21] Wang, M., Feng, Y.T., Pande, G.N., Chan, A.H.C. and Zuo, W.X., 2017. Numerical modelling of fluid-induced soil erosion in granular filters using a coupled bonded particle lattice Boltzmann method. Computers and Geotechnics, 82, pp.134-143.

[22] Wang, M., Feng, Y.T., Pande, G.N. and Zhao, T.T., 2018. A coupled 3-dimensional bonded discrete element and lattice Boltzmann method for fluid-solid coupling in cohesive geomaterials. International Journal for Numerical and Analytical Methods in Geomechanics, 42: 1405-1424.

[23] Dash, S.M., Lee, T.S., Lim, T.T. and Huang, H., 2014. A flexible forcing three dimension IB–LBM scheme for flow past stationary and moving spheres. Computers & Fluids, 95, pp.159-170.

[24] Wu, J. and Shu, C., 2009. Implicit velocity correction-based immersed boundary-lattice Boltzmann method and its applications. Journal of Computational Physics, 228(6), pp.1963-1979.

[25] Guifang, Y., Guipu, J., Lifang, Z., Shengguang, Z. and Juanxia, Z., 2011. Distribution Characteristics of Shallow Natural Gas in China Oil Fields and Its Influence on Drilling. Procedia Engineering, 26, pp.1857-1863.

[26] Omota, F., Dimian, A.C. and Bliek, A., 2006. Adhesion of solid particles to gas bubbles. Part 1: Modelling. Chemical engineering science, 61(2), pp.823-834.

[27] Wang, M., Feng, Y.T. and Pande, G.N., 2016. A coupled bonded particle and lattice Boltzmann method with its application to geomechanics. PhD, Swansea University, UK.

[28] Feng, Y.T., Han, K. and Owen, D.R.J., 2007. Coupled lattice Boltzmann method and discrete element modelling of particle transport in turbulent fluid flows: Computational issues. International Journal for Numerical Methods in Engineering, 72(9), pp.1111-1134.

[29] Wang, M., Feng, Y.T., Owen, D.R.J. and Qu, T.M., 2019. A novel algorithm of immersed moving boundary scheme for fluid–particle interactions in DEM–LBM. Computer Methods in Applied Mechanics and Engineering, 346, pp.109-125.

[30] Shang, J., Zhao, Z. and Ma, S., 2018. On the shear failure of incipient rock discontinuities under CNL and CNS boundary conditions: insights from DEM modelling. Engineering Geology, 234, pp.153-166.

[31] Tomiyama, A., 2001. (N+2)-field modeling for bubbly flow simulation. Computational Fluid Dynamics Journal, 9(4), pp.418-426.

[32] Tomiyama, A. and Shimada, N., 2001. A numerical method for bubbly flow simulation based on a multi-fluid model. Journal of pressure vessel technology, 123(4), pp.510-516.

[33] Darmana, D., Deen, N.G. and Kuipers, J.A.M., 2005. Detailed modeling of hydrodynamics, mass transfer and chemical reactions in a bubble column using a discrete bubble model. Chemical engineering science, 60(12), pp.3383-3404.

[34] Sommerfeld, M., Bourloutski, E. and Bröder, D., 2003. Euler/Lagrange calculations of bubbly flows with consideration of bubble coalescence. The Canadian Journal of Chemical Engineering, 81(3-4), pp.508-518.

[35] Darmana, D., Deen, N.G. and Kuipers, J.A.M., 2006. Parallelization of an Euler–Lagrange model using mixed domain decomposition and a mirror domain technique: Application to dispersed gas–liquid two-phase flow. Journal of Computational Physics, 220(1), pp.216-248.

[36] Lau, Y.M., Bai, W., Deen, N.G. and Kuipers, J.A.M., 2014. Numerical study of bubble break-up in bubbly flows using a deterministic Euler–Lagrange framework. Chemical Engineering Science, 108, pp.9-22.

[37] Song, C.H., Bae, B.U. and Euh, D.J., 2013. Modeling of bubble coalescence and break-up considering turbulent suppression phenomena in bubbly two-phase flow. International Journal of Multiphase Flow, 54, pp.31-42.

Figure list: